Geophysical Research Letters

RESEARCH LETTER
10.1029/2019GL085584

Orbital Identification of Hydrated Silica in Jezero Crater, Mars

J. D. Tarnas[1], J. F. Mustard[1], Honglei Lin[2], T. A. Goudge[3], E. S. Amador[4,5], M. S. Bramble[1], C. H. Kremer[1], X. Zhang[6], Y. Itoh[7], and M. Parente[7]

[1]Department of Earth, Environmental and Planetary Sciences, Brown University, Providence, RI, USA, [2]Institute of Geology and Geophysics, Chinese Academy of Sciences, Beijing, China, [3]Department of Geological Sciences, Jackson School of Geosciences, The University of Texas at Austin, Austin, TX, USA, [4]NASA Jet Propulsion Laboratory, Pasadena, CA, USA, [5]Division of Geological and Planetary Sciences, California Institute of Technology, Pasadena, CA, USA, [6]Institute of Remote Sensing and Digital Earth, Chinese Academy of Sciences, Beijing, China, [7]Department of Electrical and Computer Engineering, University of Massachusetts Amherst, Amherst, MA, USA

Key Points:
- Hydrated silica is detected in Jezero crater and could have formed in a variety of environments with different degrees of habitability
- Hydrated silica is associated with smooth dark-toned material that covers the olivine-rich unit
- Hydrated silica in Jezero crater is an excellent target for in situ investigation for biosignatures

Supporting Information:
- Supporting Information S1

Correspondence to:
J. D. Tarnas,
jesse_tarnas@brown.edu

Citation:
Tarnas, J. D., Mustard, J. F., Lin, H., Goudge, T. A., Amador, E. S., Bramble, M. S., et al. (2019). Orbital identification of hydrated silica in Jezero crater, Mars. *Geophysical Research Letters*, *46*, 12,771–12,782. https://doi.org/10.1029/2019GL085584

Received 31 JUL 2019
Accepted 1 NOV 2019
Accepted article online 6 NOV 2019
Published online 25 NOV 2019

©2019. American Geophysical Union. All Rights Reserved.

Abstract Silica has the highest demonstrated potential of any phase to preserve microfossils on Earth and therefore may host potential biosignatures on Mars. We detected hydrated silica in Jezero crater, the landing site of the National Aeronautics and Space Administration's Mars 2020 rover mission, by applying Dynamic Aperture Factor Analysis/Target Transformation to images from the Compact Reconnaissance Imaging Spectrometer for Mars. Hydrated silica detections with Dynamic Aperture Factor Analysis/Target Transformation were verified using commonly accepted Compact Reconnaissance Imaging Spectrometer for Mars analysis methods. The morphology of geologic units associated with silica was characterized with high-resolution imaging. Several hypotheses are presented for the formation environment of hydrated silica. All are testable via in situ investigation. We assess the likelihood of silica to preserve biosignatures in these different scenarios based on habitability considerations and biosignature preservation in Earth analog environments and materials. Also reported are possible detections of hydrated silica in the Nili Fossae basement and olivine-rich units, as well as Al-phyllosilicate within Jezero crater.

1. Introduction

Opaline silica (amorphous $SiO_2 \cdot nH_2O$) was first detected on Mars using the Miniature-Thermal Emission Spectrometer (Christensen et al., 2003) onboard both Mars Exploration Rovers in Meridiani Planum (Glotch et al., 2006) and Columbia Hills (Squyres et al., 2008). These detections confirmed theoretical geochemical arguments that sedimentary silica would be a common alteration product where water-rock interaction had occurred in Mars' dominantly basaltic primary crust (McLennan, 2003). More widespread outcrops of hydrated silica were identified in a variety of ancient aqueous environments using hyperspectral visible and shortwave-infrared images from the Compact Reconnaissance Imaging Spectrometer for Mars (CRISM; Murchie et al., 2007) (Bishop et al., 2008; Ehlmann et al., 2009; Fraeman et al., 2016; Milliken et al., 2008; Murchie et al., 2007; Mustard et al., 2008; Skok et al., 2010; Smith & Bandfield, 2012; Sun & Milliken, 2015, 2018). High-silica occurrences were identified with thermal infrared emissivity spectra from the Thermal Emission Spectrometer (TES; Christensen et al., 2001) and the Thermal Emission Imaging System (THEMIS; Christensen et al., 2004) (Bandfield, 2008; Bandfield et al., 2013). Both detrital and authigenic cementing silica (Morris et al., 2016) as well as silica enrichments formed by later infiltration of both alkaline and acidic fluids (Yen et al., 2017) have also been detected in Gale crater by the Mars Science Laboratory.

Formation hypotheses for silica detected on Mars include sedimentary deposition (detrital), direct precipitation (authigenic), and leaching of basaltic protolith (cation removal) (Bishop et al., 2008; Milliken et al., 2008; Ruff et al., 2011; Skok et al., 2010; Squyres et al., 2008; Yen et al., 2017). On Earth, silica forms in a wide range of settings including hot springs in both neutral-alkaline and acidic hydrothermal systems (e.g., Campbell et al., 2015), volcano-fumarolic settings (e.g., Seelos et al., 2010), marine environments (e.g., Bohrmann et al., 1994), and lacustrine settings (e.g., Eugster, 1969; Peterson & Borch, 1965). Secondary silica initially precipitates as opal-A—an amorphous phase—and becomes more crystalline upon further water-rock interaction (e.g., Kastner & Gieskes, 1983). Sun and Milliken (2018) showed that opal-A on Mars

tends to be associated with bedrock, while more crystalline silica exists primarily in unconsolidated sediments. The prevalence of opal-A on Mars has been interpreted to imply limited water-rock interaction throughout the planet's history (Tosca & Knoll, 2009).

Siliceous sinter (deposit of silica surrounding a hot spring or geyser) and chert (sedimentary microcrystalline silica) have high potential to preserve biosignatures relative to other mineral phases on Earth. This is because silicification of organic matter is caused by the bonding of silicic acid to organic cell walls and/or envelopes, causing both organic matter and morphologic biosignatures to be preserved (e.g., Knoll et al., 1985; McMahon et al., 2018). The silicification process is insensitive to variations in cell type, substrate type, pH, and salinity (McMahon et al., 2018; Orange et al., 2009, 2013, 2014). Permineralized cells, organic carbon (which may or may not appear morphologically similar to cells), molecular fossils (e.g., lipids), and microbially induced sedimentary structures are preserved exceptionally well in these mineral phases (Farmer & Des Marais, 1999; McMahon et al., 2018). Silica's rigidity, impermeability, and resistance to chemical weathering allow preserved microfossils and other biosignatures to remain relatively unaffected by external environmental conditions (McMahon et al., 2018). Determining where silica exists on the Martian surface, as well as the habitability of its various formation environments, is thus key to maximizing chances of detecting Martian biosignatures.

The Nili Fossae region is one of the most mineralogically diverse regions of Mars (Ehlmann et al., 2009; Mustard et al., 2008) and hosts a well-defined stratigraphy, including—in order from bottom to top—a Fe/Mg-phyllosilicate and Al-phyllosilicate-bearing Noachian brecciated basement unit, an olivine-enriched unit variably altered to carbonate, an olivine-poor mafic capping unit, and a locally exposed, layered sulfate-bearing unit (Ehlmann & Mustard, 2012). Jezero crater, located within the Nili Fossae region, contains some of the best preserved deltaic outcrops on Mars (Fassett & Head, 2005; Goudge et al., 2017) and once hosted an open basin lake fed by two inlet valleys from the north and west and drained through an outlet valley to the east (Goudge et al., 2015) (Figure 1c). Two deltas exist within the crater, one at each inlet channel entrance (Fassett & Head, 2005). Fassett and Head (2008) derived an age of 3.8 ± 0.1 Gyr for the Jezero valley system using buffered crater counting and the Neukum isochron system (Neukum & Hiller, 1981). This implies that fluvial activity around Jezero likely occurred during the main phase of Martian valley network formation. As Jezero crater is the landing site of the National Aeronautics and Space Administration (NASA)'s Mars 2020 rover mission, its imminent in situ investigation will enable characterization of the physical and chemical processes that occurred during the main phase of Martian valley network formation in the Noachian.

Goudge et al. (2015, 2017) generated a geomorphic map of Jezero crater and its watershed and further constrained the location of carbonate- and smectite-bearing rock units in the crater. The regionally widespread olivine-rich unit also exists within Jezero crater (Goudge et al., 2015; Kremer et al., 2019) and is no older than the ~3.96 Ga Isidis impact (Werner, 2008) and no younger than the Syrtis Major lavas that stratigraphically overlie it, which have been dated to ~3.6 Ga (Hiesinger & Head, 2004). Sedimentological evidence demonstrates the existence of an ancient lacustrine environment in Jezero crater (Fassett & Head, 2005; Goudge et al., 2017; Schon et al., 2012). The presence of carbonate in the Jezero deltas and surrounding Nili Fossae region may indicate neutral- to alkaline-pH water-rock interactions in the Jezero-hosted paleolake, the lake's watershed, and possibly the prepaleolake crater environment, favoring the existence of potentially habitable environments in all of these settings (Ehlmann et al., 2008, 2009; Goudge et al., 2015). Ehlmann et al. (2008) assessed the biosignature preservation potential of deltaic smectite clays in Jezero crater, but no study has rigorously evaluated CRISM data for the presence or absence of silica in Jezero crater or assessed its potential to host biosignatures.

2. Methods

Hydrated silica has near-infrared and shortwave-infrared absorption features at 1.37–1.46 μm (OH stretching overtones from Si-OH and H_2O), 1.91–1.96 μm (H_2O combination bending and stretching mode), and 2.21–2.26 μm (OH stretching-Si-OH bending combination mode) (Burneau et al., 1990; Sun & Milliken, 2018) (Figures S3–S6 in the supporting information). Most hydrated minerals have absorptions around 1.4 and 1.9 μm, but unique to hydrated silica is the presence, and broad shape of, the 2.21–2.26 μm absorption feature (e.g., Rice et al., 2013). An Al-OH vibrational absorption also exists near 2.2 μm but can be differentiated from the Si-OH absorption based on its shape, where the Al-OH absorption is significantly narrower

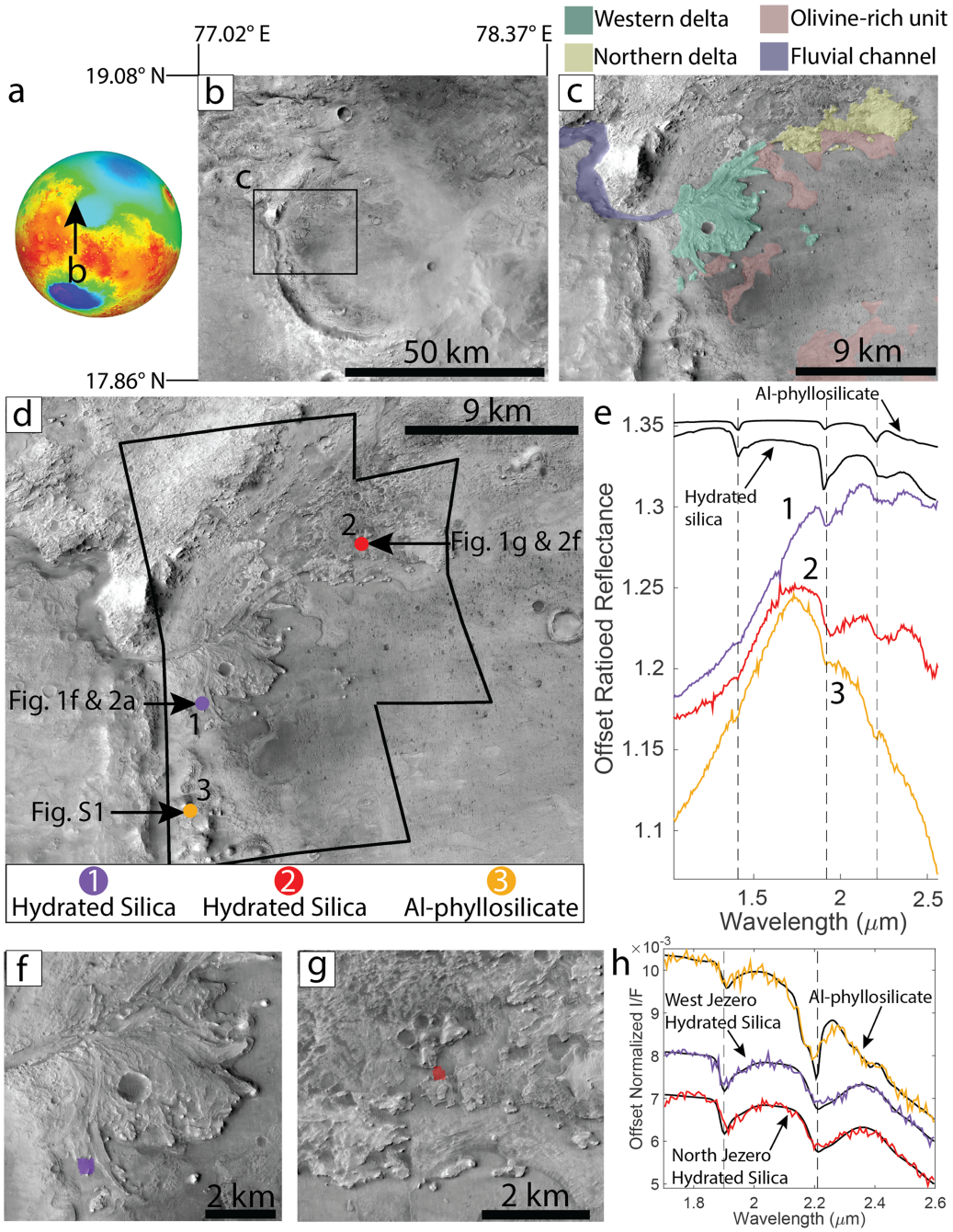

Figure 1. Overview map of Jezero crater mineralogy. (a) Location of Jezero crater on Mars globe colored with Mars Orbital Laser Altimeter topography. (b) Overview image of Jezero crater. (c) Enlarged view of western Jezero crater, with geomorphic maps from Goudge et al. (2015) of both deltas, fluvial channels, and the olivine-rich unit overlain. (d) Hydrated silica detections and an Al-phyllosilicate detection in Jezero crater generated via DAFA/TT analysis of CRISM images FRT000047A3 and HRL000040FF, with CRISM image boundaries shown in black. Detections 1 and 2 (hydrated silica) were discovered via DAFA/TT analysis and verified by extraction of ratioed spectra. Detection 3 (Al-phyllosilicate) was discovered via DAFA/TT analysis and verified by extraction of an unratioed spectrum (Figure S1). I/F spectra of each detection are shown in (e). (e) Spectra from dot locations indicated in (d), where dot colors correspond to spectra colors. Detections 1 and 2 have 2.2 μm absorptions that broaden toward longer wavelengths, as well as 1.9 and 1.4 μm absorptions (Figures S2–S5). These features indicate the presence of hydrated silica. Detection 3 is Al-phyllosilicate, based on the presence of a narrow 2.2 μm absorption accompanied by a 1.9 μm absorption (extracted from Itoh & Parente, 2019 processed CRISM image) (Figure S1). The black spectra are library spectra for hydrated silica (RELAB Spectral ID C1OP09, Sample ID OP-MCG-009) and Al-phyllosilicate (RELAB Spectral ID BIR1JB799, Sample ID JB-JLB-799), (f) Overview of hydrated silica DAFA/TT detection near the western Jezero delta (purple). (g) Overview of hydrated silica DAFA/TT detection near the northern Jezero delta (red). (h) DAFA/TT fits to library spectra for Al-phyllosilicate, hydrated silica near the western delta, and hydrated silica near the northern delta. These minerals were initially discovered via DAFA/TT analysis and then verified via extraction of I/F spectra shown in (e). The hydrated silica library spectrum for both detections is RELAB Spectral ID BKR1OP007, Sample ID OP-MCG-007. The Al-phyllosilicate library spectrum is RELAB Spectral ID BIR1JB799, Sample ID JB-JLB-799. North is up in all images.

than the Si-OH absorption (Figure 1e) (Milliken et al., 2008; Stolper, 1982). Sun and Milliken (2018) showed that the band minimum position of the 1.4 μm feature shifts to shorter wavelengths in more amorphous silica (1.37–1.42 μm) and shifts to longer wavelengths in more crystalline silica (1.41–1.44 μm). We use the presence of a 2.2 μm absorption feature with a broad shoulder toward longer wavelengths, accompanied by 1.4 and 1.9 μm absorptions, as evidence for the presence of Si-OH bonds in CRISM data, thus indicating the presence of hydrated silica where these spectral features exist.

We analyzed CRISM TRR3 (Version 3 of CRISM processing pipeline) images over Jezero crater and the surrounding Nili Fossae region that are reduced and calibrated to I/F (radiance observed by CRISM/solar radiance at Mars) using two different data processing methods. The first processing method uses the CRISM Analysis Toolkit Version 7.4 (Murchie et al., 2007) and applies standard volcano-scan atmospheric, photometric, and denoising corrections (McGuire et al., 2009). The second method applies scene-dependent atmospheric correction and denoising (Itoh & Parente, 2019). We analyzed the 1.0–2.6 μm spectral range of CRISM images FRT00005C5E, HRL000040FF, FRT000047A3, FRT00016A73, and FRT00003E12.

We used Dynamic Aperture Factor Analysis/Target Transformation (DAFA/TT) (Lin et al. 2018) to detect potential hydrated silica outcrops that were then validated using commonly applied CRISM data analysis methods of band parameter mapping and extraction of ratioed and unratioed I/F spectra. DAFA/TT, similar to previous applications of factor analysis and target transformation to CRISM data (Amador et al., 2018; Thomas & Bandfield, 2017), is capable of detecting phases present in low abundance and in complex convolutions. By spatially subsetting the CRISM data in an iterative manner, DAFA/TT is also capable of characterizing the spatial distribution of modeled minerals within a given image. Factor analysis was performed via the Hysime algorithm (Bioucas-Dias & Nascimento, 2008), which extracts the spectral endmembers that describe the signal subspace within a given set of pixels. It then performs target transformation via linear least-squares fitting of extracted signal subspace endmembers to a suite of library spectra for a variety of specific minerals (Amador et al., 2018; Bandfield et al., 2000; Glotch & Bandfield, 2006; Malinowski, 1991; Thomas & Bandfield, 2017). We perform target transformation for spectra in the 1.7–2.6 μm range in order to avoid the 1.6 μm region of CRISM, which is particularly noisy. If the target transformation fit falls below an empirically determined root-mean-square error (RMSE) threshold of 1.5×10^{-4}, we consider it a positive detection. RMSE is defined as $\sqrt{\frac{\sum_{i=1}^{n}(\hat{y}_i - y_i)^2}{n}}$ where n is the number of bands analyzed, $\hat{y}_i$ is the normalized I/F of the library spectrum at band i, and y_i is the normalized I/F of the target transformation fit at band i. Normalization is performed by dividing the I/F value at each wavelength by the sum of I/F in all wavelengths from 1.7–2.6 μm, which mitigates spectral variability caused by albedo differences in CRISM images. We perform this RMSE calculation for spectra from 1.7–2.6 μm. We applied this process to clusters of ~50 CRISM pixels with different geometries that move across the scene, shifting the center of the cluster one pixel at a time, and then only accepted pixels with detections in all cluster geometries as true detections (Lin et al., 2018). We used ~50 hydrated silica library spectra acquired from the Keck/NASA Reflectance Experiment Laboratory database as the target spectra in our CRISM image analysis, as a way to represent the significant spectral variability of this phase. The number of eigenvectors used to generate each DAFA/TT fit to library spectra is usually ≤15. The results of DAFA/TT analysis are maps used to highlight targets for subsequent investigation by commonly accepted spectral analysis methods, including band parameter mapping (e.g., Figure S6) and manual inspection of individual I/F spectra. If unratioed and ratioed spectra from those DAFA/TT highlighted pixels show a 2.2 μm absorption with a broad shape toward longer wavelengths, as well as 1.4 and 1.9 μm absorptions, we deem this a robust detection.

We determined the geologic context for the positive detections of hydrated silica and associated minerals using images from the High Resolution Imaging Science Experiment (HiRISE; McEwen et al., 2007) with a spatial resolution of ~0.25 m/pixel. Atop the HiRISE images, we used manually generated tiepoints to coregister mineral detections from the CRISM DAFA/TT analysis. These mineral maps have a spatial resolution of ~18 m/pixel (full-resolution targeted; FRT) or ~32 m/pixel (half-resolution long). We also analyzed the topographic setting of hydrated silica using HiRISE and Context Camera (Malin et al., 2007) digital elevation maps produced using the Ames Stereo Pipeline (Beyer et al., 2018; Shean et al., 2016). Most HiRISE image mosaics and digital elevation maps used in this study were generated by the Bruce Murray Lab for Planetary Visualization at the California Institute of Technology (Dickson et al., 2018).

We constrained the possible formation mechanisms for detected hydrated silica deposits by assessing their stratigraphic context and the morphological characteristics of associated rock units apparent in HiRISE images. We also used the minerals detected in association with hydrated silica to infer the geochemistry of alteration conditions that formed these silica deposits, provided that they were a product of water-rock interaction rather than primary volcanism. We base geochemical interpretations on laboratory and field studies of silica assemblage formation on Earth (e.g., Falk & Kelemen, 2015; Fialips et al., 2000; Streit et al., 2012). We also searched for exposures of hydrated silica in the olivine-rich and basement units in the greater Nili Fossae region to ascertain whether this assemblage is prevalent throughout this region of Mars.

3. Results

Both the DAFA/TT analysis (Figure 1h) and inspection of individual I/F spectra (Figures 1e, 2d, 2i, and S2–S5) indicate the presence of hydrated silica near the western and northern Jezero deltas. These detections were also reported by Dundar et al. (2019) and Parente et al. (2019). The I/F spectra for both hydrated silica detections have broad 2.2 μm absorption features, as well as a weak 1.4 μm absorption feature and stronger 1.9 μm absorption feature with band minima positions consistent with hydrated silica (Sun & Milliken, 2018) (Figures 1e, 2d, 2i, and S2–S5). Both detections of hydrated silica are likely associated with olivine and Fe/Mg-smectite based on the presence of accompanying broad 1 μm and narrow 2.3 μm absorption features (Figures 1e, 2d, 2i, and S3–S6) in both hydrated silica spectra. We also detected possible hydrated silica in the olivine-rich unit elsewhere in the Nili Fossae region, where it is associated with olivine, magnesite, and Fe/Mg-smectite (Figures 3e–3g). This is based on the presence of a 2.2 μm shoulder accompanied by broad 1 μm, narrow 2.3 μm, narrow 2.39 μm, and narrow 2.5 μm absorption features (Figure 3g). Additionally, hydrated silica is detected in the basement unit, the oldest unit in the exposed Nili Fossae stratigraphy (Bramble et al., 2017), based on the presence of a broad 2.2 μm absorption feature accompanied by 1.4 and 1.9 μm absorption features. This hydrated silica is associated with Al-phyllosilicate (Figure 3d) based on the presence of a narrow absorption feature centered at 2.2 μm and accompanied by 1.4 and 1.9 μm absorption features. Because we have detected hydrated silica in the basement unit and possible hydrated silica in the olivine-rich unit, which are the units incised by the fluvial channels in Jezero's watershed (Goudge et al., 2015), we refer to these as possible hydrated silica detections in the Jezero watershed *rock units*.

Both detections of hydrated silica in Jezero crater are associated with dark-toned material that covers the olivine-rich unit. The olivine-rich unit can be seen protruding through the smooth dark-toned material in some areas. The dark-toned material appears smooth at the scale of HiRISE and is covered in some areas by aeolian bedforms (Figures 2e and 2j). Delta remnants surround the hydrated silica detections on the north and south sides (Figures 2a–2c and 2f–2h). There is no geomorphic evidence for the existence of the volcanic floor unit in this area, which stratigraphically overlies the delta remnants (Goudge et al., 2015), and indeed, the observed silica-bearing smooth dark-toned material does not contain the large fractures and numerous small impact craters typically found in the volcanic floor unit as defined by Goudge et al. (2015) (Figures 2e and 2j). The olivine-rich unit is exposed from beneath the smooth dark-toned material cover southeast of the hydrated silica detection near the western delta and northeast of the hydrated silica detection near the northern delta.

Al-phyllosilicate is detected with DAFA/TT near a mound south of the western Jezero delta (Figure S1), and its presence is verified via extraction of spectra that exhibit a narrow 2.2 μm absorption feature accompanied by 1.4 and 1.9 μm absorption features. There is also a 2.3 μm absorption feature associated with the Al-phyllosilicate, indicating that it is mixed with Fe/Mg-smectite. Magnesite and Fe/Mg-smectite are associated with both the delta and the olivine-rich unit in Jezero crater (Ehlmann et al., 2009; Goudge et al., 2015, 2017), in contrast to hydrated silica which is primarily associated with dark-toned material that covers the olivine-rich unit and is smooth at the scale of HiRISE spatial resolution. These new detections of hydrated silica and Al-phyllosilicate increase the mineral diversity observed within Jezero crater that similarly resembles that observed in the greater Nili Fossae region (Ehlmann et al., 2009), which includes the watershed for the Jezero deltas.

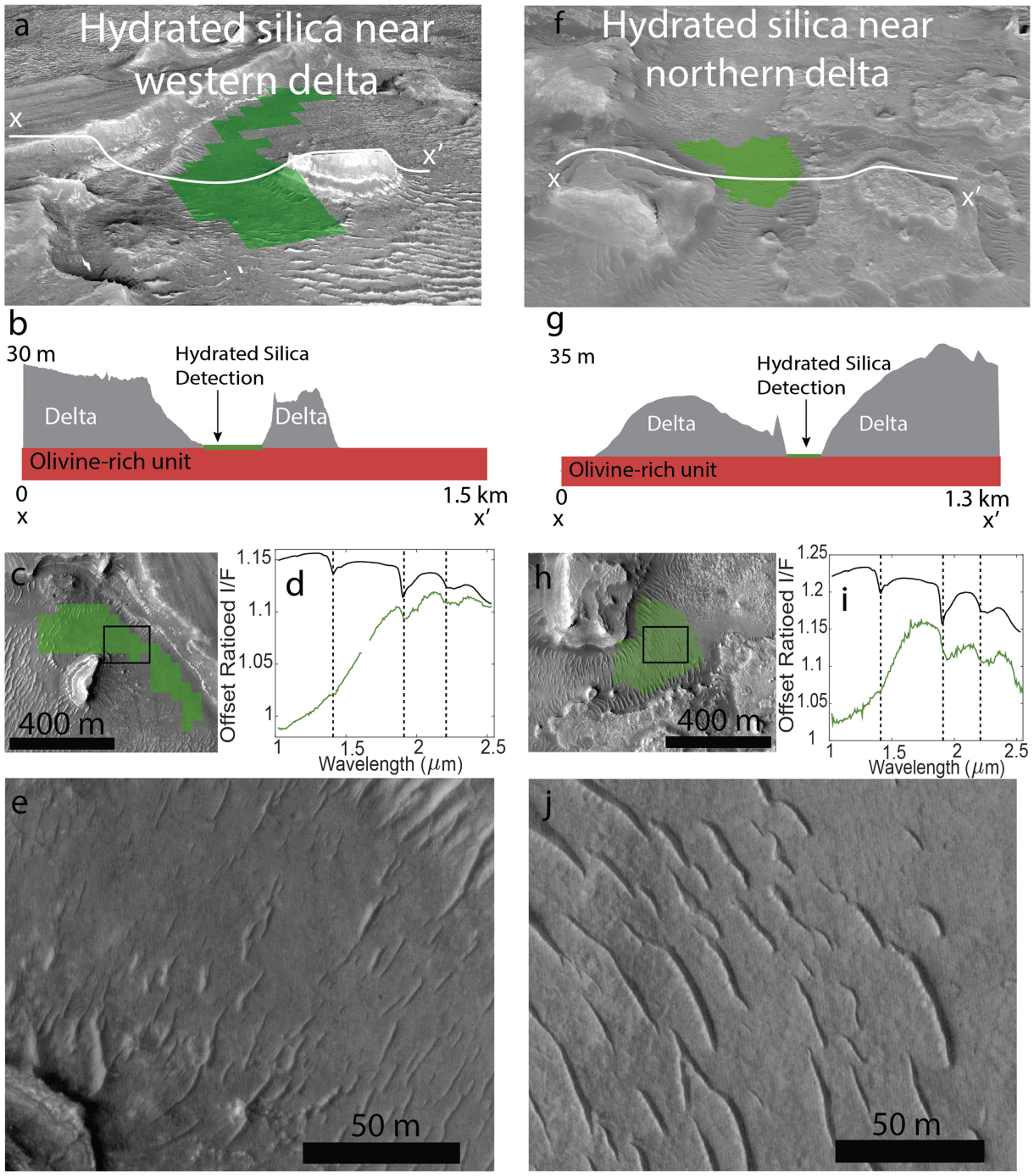

Figure 2. Hydrated silica detections in Jezero crater. (a) Hydrated silica detection (green) near the western delta overlain on HiRISE DEM and images. The white line denotes the elevation profile cross section shown in (b). (b) Elevation profile from cross section shown in (a) illustrating the relationship between the elevation profile, silica detection, olivine-rich unit, and deltaic unit. (c) Location of hydrated silica detected near western Jezero delta (green). The rectangle shows the area that is enlarged in part (e). (d) (black) Library spectrum of hydrated silica (RELAB Spectral ID C1OP09, Sample ID OP-MCG-009). (green) Ratio spectrum of hydrated silica near western delta from green pixels in (a) and (c). The dotted lines are at 1.41, 1.93, and 2.21 μm. (e) Enlarged view of hydrated silica detection near the western delta. The linear features are aeolian bedforms. The underlying smooth dark-toned material bears the hydrated silica spectral signal. (f) Hydrated silica detection (green) near the northern delta overlain on CTX DEM and HiRISE images. The white line denotes the elevation profile cross section shown in (g). (g) Elevation profile from cross section shown in (f) illustrating the relationship between the elevation profile, silica detection, olivine-rich unit, and deltaic unit. (h) Location of hydrated silica detected near northern delta (green). The rectangle shows the area that is enlarged in part (j). (i) (black) Library spectrum of hydrated silica (RELAB Spectral ID C1OP09, Sample ID OP-MCG-009). (green) Ratioed spectrum of hydrated silica near northern delta from green pixels in (f) and (h). The dotted lines are at 1.41, 1.93, and 2.21 μm. (j) Enlarged view of hydrated silica detection near the northern delta. The linear features are aeolian bedforms. The underlying smooth dark-toned material bears the hydrated silica spectral signal. North is up in parts (c)–(e) and (h)–(j). North is to the left in parts (a) and (f).

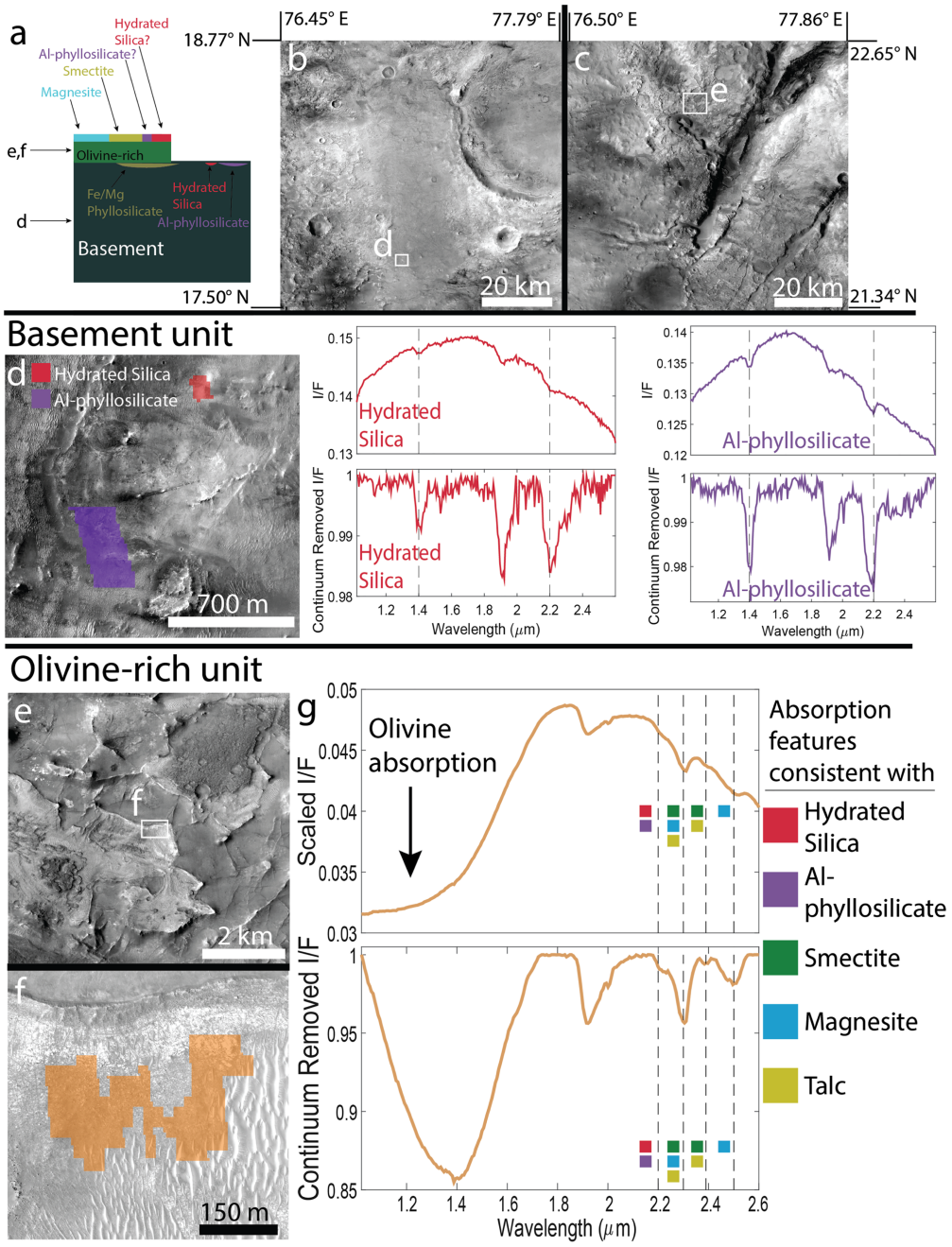

Figure 3. Hydrated silica and associated minerals detected in Jezero watershed rock units. (a) Conceptual stratigraphic cross section showing relationship between Nili Fossae basement unit and overlying olivine-rich unit, with detected alteration minerals shown. (b) Overview of circum-Jezero region. (c) Overview of other location in Nili Fossae where hydrated silica is detected in the olivine-rich unit. (d) Detection of Al-phyllosilicate (purple) and hydrated silica (red) in the basement unit. The purple spectrum is from the purple pixels, and the red spectrum is from the red pixels. The presence of hydrated silica is indicated by the presence of 1.4, 1.9, and 2.2 μm absorptions, where the 2.2 μm absorption broadens toward longer wavelengths. The presence of Al-phyllosilicate is indicated by the presence of 1.4, 1.9, and 2.2 μm absorptions, where the 2.2 μm absorption is significantly narrower than that of hydrated silica. Spectra are shown in standard I/F and in continuum removed I/F. Presence of this mineral assemblage is possibly indicative of acidic hydrothermal alteration. (e) Overview of area where possible hydrated silica is detected in the olivine-rich unit. (f) Enlarged view of olivine-rich unit with its characteristic fractured texture. The orange pixels contain the spectral signal shown in (g). (g) Hydrated silica or Al-phyllosilicate detected in assemblage with magnesite and smectite or talc. The orange spectrum is from the orange pixels in (f). The spectrum is shown in standard I/F and in continuum removed I/F. the broad absorption feature centered at 1 μm is indicative of olivine. It appears to be centered at 1.4 μm in the continuum removed spectrum because the continuum starts at 1.03 μm due to the wavelength range of the CRISM long wavelength detector (1.03–3.92 μm). Boxes near dotted lines going through absorptions at 2.2, 2.3, 2.39, and 2.5 μm indicate the minerals with which these absorption features are consistent. The 2.3 and 2.39 μm features are also present in talc, so hydrated silica/Al-phyllosilicate may be associated with magnesite and talc rather than magnesite and smectite. North is up in all images. All spectra shown in this figure were extracted from CRISM TRR3 images processed through the pipeline described in Itoh and Parente et al. (2019).

4. Discussion

We cannot discern whether the hydrated silica in Jezero crater is opal-A or opal-CT via the method of Sun and Milliken (2018), which uses the band minimum position of the 1.4 μm feature to estimate crystallinity of silica. The 1.4 μm features in our spectra are quite weak, making it difficult to interpret the crystallinity of these samples. Laboratory studies show that the weakness of the 1.4 μm absorption feature in some hydrated silica spectra can be attributed to the dehydration of silica through either heating or exposure to a Mars analog atmosphere, as has been witnessed in other hydrated silica spectra on Mars (e.g., Skok et al., 2010). The hydrated silica detection near the northern delta has a 1.4 μm feature with a band minimum at 1.41 μm (Figures S3 and S4), which can be attributed to either opal-A or opal-CT via the method of Sun and Milliken (2018). The ratioed spectrum for the hydrated silica near the western delta has a 1.4 μm feature centered near 1.42 μm, which indicates that it is closer in crystallinity to opal-CT than opal-A based on the findings of Sun and Milliken (2018), but is not uniquely diagnostic of either opal-A or opal-CT. As such, the crystallinity of this silica cannot be used to constrain the amount of water-rock interaction experienced by this phase, in contrast to hydrated silica detected elsewhere on Mars (Morris et al., 2016; Sun & Milliken, 2018).

Hydrated silica detected by rovers on Mars likely formed in a variety of geochemical conditions, which varied widely in their degrees of habitability. The Spirit rover discovered opaline silica that likely formed as a hot spring sinter deposit (Ruff & Farmer, 2016), while the Curiosity rover discovered detrital silica, silica formed as a cement (Morris et al., 2016), as well as silica enrichments formed via infiltration of alkaline fluids that transitioned to acidic fluids (Yen et al., 2017). Fine-grained and/or amorphous silica formed by water-rock interaction is an exceptional material for preserving biosignatures on Earth and therefore has high biosignature preservation *potential*. Constraining the types of geochemical environments in which hydrated silica in Jezero crater could have formed is key to assessing these environments' habitability and thus the likelihood of this silica to host biosignatures.

The geochemical origin and provenance of the dark-toned material associated with hydrated silica—which covers the olivine-rich unit and appears smooth at HiRISE spatial resolution—is ambiguous. The silica-bearing smooth dark-toned material appears to occur exclusively in close proximity to the delta remnants (Figures 1f, 1g, 2a, and 2f). It may represent the stratigraphically lowest component of the deltaic unit, as the olivine-rich unit protrudes through it and directly underlies it at multiple contacts visible in HiRISE images (Figures 2c, 2e, and 2h). Alternatively, it may be colluvial material that has been sourced from the breakdown of the adjacent deltaic outcrops. It is unlikely that the spectral signature for hydrated silica comes primarily from the aeolian bedforms overlying the smooth dark-toned material, as these bedforms cover a minor proportion of the CRISM pixels used to generate the hydrated silica spectra from near the northern and western deltas (Figures 2a, 2c, 2e, 2f, 2h, and 2j) relative to the smooth dark-toned material. The aeolian bedforms cover an especially small area in the CRISM pixels used to generate the hydrated silica spectrum near the western delta (Figure 2e). Therefore, we hypothesize that the silica is most likely associated with the smooth dark-toned material rather than the overlying aeolian bedforms.

If the smooth dark-toned material associated with hydrated silica is the stratigraphically lowest component of the deltaic unit, then deltaic hydrated silica is present in Jezero crater. If this potential deltaic hydrated silica is an alteration product, it could have formed authigenically in three possible scenarios: (1) via precipitation during formation of the western and northern deltas (silica is cement); (2) precipitation in the lake water column (silica is in fine sediment grains within the cementing matrix), which may have also occurred in Gale crater (Morris et al., 2016); or (3) later diagenesis via fluid infiltration, as seen in Gale crater (Yen et al., 2017). Alternatively, it could be detrital material that formed in the Jezero watershed in either (1) a neutral-pH hydrothermal system or (2) an acidic hydrothermal system, such as those hypothesized to exist based on the mineral assemblages detected in the Jezero watershed rock units (Figures 3d–3g). If this silica is hydrated volcanic glass, it could have been deposited within the Jezero watershed and would have remained undissolved during fluvial transport, which is theoretically possible in cold, acidic, silica-saturated solutions. Alternatively, it could be hydrated volcanic glass-bearing material transported to its current location via aeolian processes. All formation hypotheses for detected silica are presented in Table S1.

Possible hydrated silica in the Jezero watershed rock units is present in association with magnesite and Fe/Mg-smectite in the olivine-rich unit (Figures 3e–3g)—favoring formation in neutral-pH hydrothermal

conditions (e.g., Falk & Kelemen, 2015; Streit et al., 2012)—as well as in association with Al-phyllosilicate in the Noachian basement unit (Figure 3d), favoring formation in highly acidic hydrothermal conditions (Fialips et al., 2000). As such, none of the detrital origin hypotheses can be ruled out for the hydrated silica in Jezero crater. Similarly, none of the authigenic hypotheses nor the primary volcanic hypotheses for hydrated silica's origin can be ruled out either. In situ investigation is therefore necessary to distinguish between these possible formation scenarios. We evaluated some of the in situ observations that would be consistent with each origin hypothesis in Table S1.

The various geochemical conditions implied by the proposed formation hypotheses for hydrated silica in Jezero crater span from uninhabitable with no chance for biosignature preservation, to habitable with high likelihood to preserve biosignatures (Table S1), if life existed in Jezero crater's lake, in an ancient hydrothermal system in Jezero crater, or elsewhere in the Jezero watershed. Earth analog environments and materials can be used to assess where biosignatures in silica would likely be found for each different origin hypothesis that involves habitable geochemical conditions. Authigenic silica cements preserve 3.4 Gyr old microfossils in the Strelley Pool Formation in Western Australia (Wacey et al., 2011). Such silica cements are the types of materials where biosignatures could be hosted in possible deltaic secondary silica in Jezero crater, if this material formed via authigenic hypotheses 1 or 2. Detrital silica sediments preserve Proterozoic age microfossils in bedded cherts found in the Buxa Formation in Northeast India (Schopf et al., 2008). This scenario, where microfossils are preserved in detrital silica sediment grains rather than the cementing matrix, is analogous to where biosignatures from detrital silica could be located in possible deltaic hydrated silica in Jezero crater or in silica that formed in a habitable environment and was transported to Jezero crater via aeolian processes.

Hydrated silica formed via alteration of preexisting units in Jezero crater during a later diagenetic event (authigenic hypothesis 3) has the potential to preserve biosignatures, given that it could have formed in water-rock alteration systems with a wide range of possible temperatures and pHs. Earth analogs in which ancient microfossils are preserved in silica also exist for this scenario. For example, silica precipitated in subsurface hydrothermal systems (not in surficial hot springs) preserves 3.5 Gyr old kerogen biosignatures in the North Pole area, Western Australia (Ueno et al., 2004). Silica associated with smooth dark-toned material in Jezero crater may be associated with smectite, but this assemblage is not indicative of any particular pH during silica formation. Overall, hydrated silica detected in Jezero crater is an excellent target for in situ astrobiological investigation, if it is secondary rather than volcanic in origin. However, the possibility of a volcanic origin for this silica cannot be ruled out from orbit; thus, in situ investigation is required to fully constrain the likelihood of this material to host biosignatures.

5. Conclusions

We have detected occurrences of hydrated silica in Jezero crater associated with dark-toned material that covers the olivine-rich unit and appears morphologically smooth at HiRISE spatial resolution. From orbit, we cannot definitively determine whether this silica is hydrated volcanic glass or a secondary alteration product. Possible hydrated silica was detected in the Jezero watershed rock units, in both the olivine-rich unit and the basement unit (Figures 3d–3g). In the olivine-rich unit, possible hydrated silica is associated with magnesite and smectite, whereas in the basement unit, it is associated with Al-phyllosilicate. We interpret the former mineral assemblage to be indicative of neutral- to alkaline-pH alteration conditions and interpret the latter mineral assemblage to be indicative of acidic alteration conditions (Falk & Kelemen, 2015; Fialips et al., 2000; Streit et al., 2012).

The likelihood of detected silica to host biosignatures is highly dependent on the geochemical conditions of its formation environment. We have proposed nine hypotheses for the origin of hydrated silica in Jezero crater, including primary volcanism, diagenesis via fluid infiltration of the olivine-rich or deltaic units, authigenic formation in a lacustrine environment, detrital transport of material formed authigenically in the Jezero watershed, or transport to Jezero crater via aeolian processes. We are limited in our ability to further constrain these formation hypotheses from orbit, but with imminent in situ exploration of this area by NASA's Mars 2020 rover mission, we will soon be able to more accurately constrain the origin of this detected silica and thus can assess its likelihood to preserve biosignatures with greater confidence, precision, and accuracy.

Data Availability Statement

The data sets used in this study are available on Harvard Dataverse.

Author Contributions

J. D. T. and H. L. developed DAFA/TT with primary advisement from J. F. M., advisement from X. Z., and feedback from E. S. A. that improved the method. J. D. T. used DAFA/TT to detect hydrated silica and used traditional CRISM data analysis to verify the detection, and wrote the manuscript. T. A. G. provided input regarding the geologic units associated with silica and geomorphological interpretations. C. H. K. and M. S. B. helped significantly with geomorphologic interpretations and figure development. Y. I. and M. P. processed CRISM images through their pipeline to cross-verify detections and generate more easily interpretable data. All authors contributed to the interpretation and final version of the manuscript.

Acknowledgments
We thank Steve Ruff and David Des Marais for thorough and thoughtful reviews that significantly improved the quality of the manuscript. We thank Vivian Sun for comments and discussion that improved the quality of this manuscript. We thank Ralph Milliken for many useful discussions. We thank the CRISM "Fandango" data analysis working group for helping to verify our hydrated silica detections, especially Frank Seelos and Raymond Arvidson. We thank Jay Dickson and The Murray Lab at Caltech for providing CTX and HiRISE mosaics. We thank the MRO team for the proposal, development, and execution of the mission that collected the data used here. Partial support to J. F. M. and J. D. T. via Grant NNX13AK72G through the NASA Mars Data Analysis Program is gratefully acknowledged.

References

Amador, E. S., Bandfield, J. L., & Thomas, N. H. (2018). A search for minerals associated with serpentinization across Mars using CRISM spectral data. *Icarus*, *311*, 113–134. https://doi.org/10.1016/j.icarus.2018.03.021

Bandfield, J. L. (2008). High-silica deposits of an aqueous origin in western Hellas Basin, Mars. *Geophysical Research Letters*, *35*, L12205. https://doi.org/10.1029/2008GL033807

Bandfield, J. L., Amador, E. S., & Thomas, N. H. (2013). Extensive hydrated silica materials in western Hellas Basin, Mars. *Icarus*, *226*(2), 1489–1498. https://doi.org/10.1016/j.icarus.2013.08.005

Bandfield, J. L., Christensen, P. R., & Smith, M. D. (2000). Spectral data set factor analysis and end-member recovery: Application to analysis of Martian atmospheric particulates. *Journal of Geophysical Research*, *105*(E4), 9573–9587. https://doi.org/10.1029/1999JE001094

Beyer, R. A., Alexandrov, O., & McMichael, S. (2018). The Ames Stereo Pipeline: NASA's open source software for deriving and processing terrain Data. *Earth and Space Science*, *5*(9), 537–548. https://doi.org/10.1029/2018EA000409

Bioucas-Dias, J. M., & Nascimento, J. M. P. (2008). Hyperspectral subspace identification. *IEEE Transactions on Geoscience and Remote Sensing*, *46*(8), 2435–2445. https://doi.org/10.1109/TGRS.2008.918089

Bishop, J. L., Dobrea, E. Z. N., McKeown, N. K., Parente, M., Ehlmann, B. L., Michalski, J. R., et al. (2008). Phyllosilicate diversity and past aqueous activity revealed at Mawrth Vallis, Mars. *Science*, *321*(5890), 830–833. https://doi.org/10.1126/science.1159699

Bohrmann, G., Abelmann, A., Gersonde, R., Hubberten, H., & Kuhn, G. (1994). Pure siliceous ooze, a diagenetic environment for early chert formation. *Geology*, *22*(3), 207–210. https://doi.org/10.1130/0091-7613(1994)022<0207:PSOADE>2.3.CO;2

Bramble, M. S., Mustard, J. F., & Salvatore, M. R. (2017). The geological history of Northeast Syrtis Major, Mars. *Icarus*, *293*, 66–93. https://doi.org/10.1016/j.icarus.2017.03.030

Burneau, A., Barres, O., Gallas, J. P., & Lavalley, J. C. (1990). Comparative study of the surface hydroxyl groups of fumed and precipitated silicas. 2. Characterization by infrared spectroscopy of the interactions with water. *Langmuir*, *6*(8), 1364–1372. https://doi.org/10.1021/la00098a008

Campbell, K. A., Guido, D. M., Gautret, P., Foucher, F., Ramboz, C., & Westall, F. (2015). Geyserite in hot-spring siliceous sinter: Window on Earth's hottest terrestrial (paleo)environment and its extreme life. *Earth-Science Reviews*, *148*, 44–64. https://doi.org/10.1016/j.earscirev.2015.05.009

Christensen, P. R., Bandfield, J. L., Hamilton, V. E., Ruff, S. W., Kieffer, H. H., Titus, T. N., et al. (2001). Mars Global Surveyor Thermal Emission Spectrometer experiment: Investigation description and surface science results. *Journal of Geophysical Research*, *106*(E10), 23,823–23,871. https://doi.org/10.1029/2000JE001370

Christensen, P. R., Jakosky, B. M., Kieffer, H. H., Malin, M. C., McSween, Jr, H. Y., Nealson, K., et al. (2004). The Thermal Emission Imaging System (THEMIS) for the Mars 2001 Odyssey Mission. *Space Science Reviews*, *110*(1/2), 85–130. https://doi.org/10.1023/B:SPAC.0000021008.16305.94

Christensen, P. R., Mehall, G. L., Silverman, S. H., Anwar, S., Cannon, G., Gorelick, N., et al. (2003). Miniature thermal emission spectrometer for the Mars Exploration Rovers. *Journal of Geophysical Research*, *108*(E12), 8064. https://doi.org/10.1029/2003JE002117

Dickson, J. L., Kerber, L. A., Fassett, C. I., & Ehlmann, B. L. (2018). A global blended CTX mosaic of Mars with vectorized seam mapping: a new mosaicking pipeline using principles of non-destructive image editing, 49th Lunar and Planetary Science Conference, The Woodlands, TX, March 19-23, 2018, Abstract 2480.

Dundar, M., Ehlmann, B. L., & Leask, E. (2019). Rare phase detections in CRISM data at pixel-scale by machine learning generate new discoveries about geology at Mars rover landing areas: Jezero and NE Syrtis, 50th *LPSC* , 3105.

Ehlmann, B. L., & Mustard, J. F. (2012). An in-situ record of major environmental transitions on early Mars at Northeast Syrtis Major. *Geophysical Research Letters*, *39*, L11202. https://doi.org/10.1029/2012GL051594

Ehlmann, B. L., Mustard, J. F., Fassett, C. I., Schon, S. C., Head, J. W. III, Des Marais, D. J., et al. (2008). Clay minerals in delta deposits and organic preservation potential on Mars. *Nature Geoscience*, *1*(6), 355–358. https://doi.org/10.1038/ngeo207

Ehlmann, B. L., Mustard, J. F., Swayze, G. A., Clark, R. N., Bishop, J. L., Poulet, F., et al. (2009). Identification of hydrated silicate minerals on Mars using MRO-CRISM: Geologic context near Nili Fossae and implications for aqueous alteration. *Journal of Geophysical Research*, *114*, E00D08. https://doi.org/10.1029/2009JE003339

Eugster, H. P. (1969). Inorganic bedded cherts from the Magadi area, Kenya. *Contributions to Mineralogy and Petrology*, *22*(1), 1–31. https://doi.org/10.1007/BF00388011

Falk, E. S., & Kelemen, P. B. (2015). Geochemistry and petrology of listvenite in the Samail ophiolite, Sultanate of Oman: Complete carbonation of peridotite during ophiolite emplacement. *Geochimica et Cosmochimica Acta*, *160*, 70–90. https://doi.org/10.1016/j.gca.2015.03.014

Farmer, J. D., & Des Marais, D. J. (1999). Exploring for a record of ancient Martian life. *Journal of Geophysical Research*, *104*(E11), 26,977–26,995. https://doi.org/10.1029/1998JE000540

Fassett, C. I., & Head, J. W. (2005). Fluvial sedimentary deposits on Mars: Ancient deltas in a crater lake in the Nili Fossae region. *Geophysical Research Letters*, *32*, L14201. https://doi.org/10.1029/2005GL023456

Fassett, C. I., & Head, J. W. (2008). The timing of Martian valley network activity: Constraints from buffered crater counting. *Icarus*, *195*(1), 61–89. https://doi.org/10.1016/j.icarus.2007.12.009

Fialips, C.-I., Petit, S., Decarreau, A., & Beaufort, D. (2000). Influence of synthesis pH on kaolinite "crystallinity" and surface properties. *Clays and Clay Minerals*, *48*(2), 173–184.

Fraeman, A. A., Ehlmann, B. L., Arvidson, R. E., Edwards, C. S., Grotzinger, J. P., Milliken, R. E., et al. (2016). The stratigraphy and evolution of lower Mount Sharp from spectral, morphological, and thermophysical orbital data sets. *Journal of Geophysical Research: Planets*, *121*, 1713–1736. https://doi.org/10.1002/2016JE005095

Glotch, T. D., & Bandfield, J. L. (2006). Determination and interpretation of surface and atmospheric Miniature Thermal Emission Spectrometer spectral end-members at the Meridiani Planum landing site. *Journal of Geophysical Research*, *111*, E12S06. https://doi.org/10.1029/2005JE002671

Glotch, T. D., Bandfield, J. L., Christensen, P. R., Calvin, W. M., McLennan, S. M., Clark, B. C., et al. (2006). Mineralogy of the light-toned outcrop at Meridiani Planum as seen by the Miniature Thermal Emission Spectrometer and implications for its formation. *Journal of Geophysical Research*, *111*, E12S03. https://doi.org/10.1029/2005JE002672

Goudge, T. A., Milliken, R. E., Head, J. W., Mustard, J. F., & Fassett, C. I. (2017). Sedimentological evidence for a deltaic origin of the western fan deposit in Jezero crater, Mars and implications for future exploration. *Earth and Planetary Science Letters*, *458*, 357–365. https://doi.org/10.1016/j.epsl.2016.10.056

Goudge, T. A., Mustard, J. F., Head, J. W., Fassett, C. I., & Wiseman, S. M. (2015). Assessing the mineralogy of the watershed and fan deposits of the Jezero crater paleolake system, Mars. *Journal of Geophysical Research: Planets*, *120*, 775–808. https://doi.org/10.1002/2014JE004782

Hiesinger, H., & Head, J. W. (2004). The Syrtis Major volcanic province, Mars: Synthesis from Mars Global Surveyor data. *Journal of Geophysical Research*, *109*, E01004. https://doi.org/10.1029/2003JE002143

Itoh, Y. & Parente, M. (2019) A new simultaneous atmospheric correction and de-noising of CRISM data, 50th LPSC, 2025.

Kastner, M., & Gieskes, J. M. (1983). Chapter 13 opal-A to opal-Ct transformation: A kinetic study. In A. Iijima, J. R. Hein, & R. Siever (Eds.), *Developments in Sedimentology* (Vol. 36, pp. 211–227). Amsterdam: Elsevier. https://doi.org/10.1016/S0070-4571(08)70092-X

Knoll, A. H., Whittington, H. B., & Morris, S. C. (1985). Exceptional preservation of photosynthetic organisms in silicified carbonates and silicified peats. *Philosophical Transactions of the Royal Society of London. B, Biological Sciences*, *311*(1148), 111–122. https://doi.org/10.1098/rstb.1985.0143

Kremer, C. H., Mustard, J. F., & Bramble, M. S. (2019). A widespread olivine-rich ash deposit on Mars. *Geology*, *47*(7), 677–681.

Lin, H., Tarnas, J. D., Mustard, J. F., Zhang, X., & Wu, X. (2018). Dynamic Aperture Target Transformation (DATT): A novel and valuable method for mineral detection on Mars, 49th Lunar and Planetary Science Conference, The Woodlands, TX, March 19-23, 2018, Abstract 1835.

Malin, M. C., Bell, J. F. III, Cantor, B. A., Caplinger, M. A., Calvin, W. M., Clancy, R. T., et al. (2007). Context camera investigation on board the Mars Reconnaissance Orbiter. *Journal of Geophysical Research*, *112*, E05S04. https://doi.org/10.1029/2006JE002808

Malinowski, E. R. (1991). Factor analysis in chemistry. Retrieved from https://www.bcin.ca/bcin/detail.app?id = 419178

McEwen, A. S., Eliason, E. M., Bergstrom, J. W., Bridges, N. T., Hansen, C. J., Delamere, W. A., et al. (2007). Mars Reconnaissance Orbiter's High Resolution Imaging Science Experiment (HiRISE). *Journal of Geophysical Research*, *112*, E05S02. https://doi.org/10.1029/2005JE002605

McGuire, P. C., Bishop, J. L., Brown, A. J., Fraeman, A. A., Marzo, G. A., Frank Morgan, M., et al. (2009). An improvement to the volcano-scan algorithm for atmospheric correction of CRISM and OMEGA spectral data. *Planetary and Space Science*, *57*(7), 809–815. https://doi.org/10.1016/j.pss.2009.03.007

McLennan, S. M. (2003). Sedimentary silica on Mars. *Geology*, *31*(4), 315–318. https://doi.org/10.1130/0091-7613(2003)031<0315:SSOM>2.0.CO;2

McMahon, S., Bosak, T., Grotzinger, J. P., Milliken, R. E., Summons, R. E., Daye, M., et al. (2018). A field guide to finding fossils on Mars. *Journal of Geophysical Research: Planets*, *123*, 1012–1040. https://doi.org/10.1029/2017JE005478

Milliken, R. E., Swayze, G. A., Arvidson, R. E., Bishop, J. L., Clark, R. N., Ehlmann, B. L., et al. (2008). Opaline silica in young deposits on Mars. *Geology*, *36*(11), 847–850. https://doi.org/10.1130/G24967A.1

Morris, R. V., Vaniman, D. T., Blake, D. F., Gellert, R., Chipera, S. J., Rampe, E. B., et al. (2016). Silicic volcanism on Mars evidenced by tridymite in high-SiO_2 sedimentary rock at Gale crater. *Proceedings of the National Academy of Sciences*, *113*(26), 7071–7076. https://doi.org/10.1073/pnas.1607098113

Murchie, S., Arvidson, R., Bedini, P., Beisser, K., Bibring, J. P., Bishop, J., et al. (2007). Compact Reconnaissance Imaging Spectrometer for Mars (CRISM) on Mars Reconnaissance Orbiter (MRO). *Journal of Geophysical Research*, *112*, E05S03. https://doi.org/10.1029/2006JE002682

Mustard, J. F., Murchie, S. L., Pelkey, S. M., Ehlmann, B. L., Milliken, R. E., Grant, J. A., et al. (2008). Hydrated silicate minerals on Mars observed by the Mars Reconnaissance Orbiter CRISM instrument. *Nature*, *454*(7202), 305–309. https://doi.org/10.1038/nature07097

Neukum, G., & Hiller, K. (1981). Martian ages. *Journal of Geophysical Research*, *86*(B4), 3097–3121. https://doi.org/10.1029/JB086iB04p03097

Orange, F., Westall, F., Disnar, J.-R., Prieur, D., Bienvenu, N., Romancer, M. L., & Défarge, C. (2009). Experimental silicification of the extremophilic Archaea Pyrococcus abyssi and Methanocaldococcus jannaschii: Applications in the search for evidence of life in early Earth and extraterrestrial rocks. *Geobiology*, *7*(4), 403–418. https://doi.org/10.1111/j.1472-4669.2009.00212.x

Orange, F., Dupont, S., Goff, O. L., Bienvenu, N., Disnar, J.-R., Westall, F., & Romancer, M. L. (2014). Experimental fossilization of the thermophilic Gram-positive bacterium Geobacillus SP7A: A long duration preservation study. *Geomicrobiology Journal*, *31*(7), 578–589. https://doi.org/10.1080/01490451.2013.860208

Orange, F., Lalonde, S. V., & Konhauser, K. O. (2013). Experimental simulation of evaporation-driven silica sinter formation and microbial silicification in hot spring systems. *Astrobiology*, *13*(2), 163–176. https://doi.org/10.1089/ast.2012.0887

Parente, M., Arvidson, R., Itoh, Y., Lin, H., Mustard, J.F., Saranathan, A.M., et al. (2019) Mineral detections over Jezero crater using advanced data processing techniques for CRISM data–the CRISM "Fandango", *Ninth International Conference on Mars*, 6382.

Peterson, M. N. A., & Borch, C. C. V. D. (1965). Chert: Modern inorganic deposition in a carbonate-precipitating locality. *Science*, *149*(3691), 1501–1503. https://doi.org/10.1126/science.149.3691.1501

Rice, M. S., Cloutis, E. A., Bell, J. F. III, Bish, D. L., Horgan, B. H., Mertzman, S. A., et al. (2013). Reflectance spectra diversity of silica-rich materials: Sensitivity to environment and implications for detections on Mars. *Icarus*, *223*(1), 499–533. https://doi.org/10.1016/j.icarus.2012.09.021

Ruff, S. W., & Farmer, J. D. (2016). Silica deposits on Mars with features resembling hot spring biosignatures at El Tatio in Chile. *Nature Communications*, *7*, 13,554. https://doi.org/10.1038/ncomms13554

Ruff, S. W., Farmer, J. D., Calvin, W. M., Herkenhoff, K. E., Johnson, J. R., Morris, R. V., et al. (2011). Characteristics, distribution, origin, and significance of opaline silica observed by the Spirit rover in Gusev crater, Mars. *Journal of Geophysical Research*, *116*, E00F23. https://doi.org/10.1029/2010JE003767

Schon, S. C., Head, J. W., & Fassett, C. I. (2012). An overfilled lacustrine system and progradational delta in Jezero crater, Mars: Implications for Noachian climate. *Planetary and Space Science*, *67*(1), 28–45. https://doi.org/10.1016/j.pss.2012.02.003

Schopf, J. W., Tewari, V. C., & Kudryavtsev, A. B. (2008). Discovery of a new chert-permineralized microbiota in the Proterozoic Buxa Formation of the Ranjit window, Sikkim, Northeast India, and its astrobiological implications. *Astrobiology*, *8*(4), 735–746. https://doi.org/10.1089/ast.2007.0184

Seelos, K. D., Arvidson, R. E., Jolliff, B. L., Chemtob, S. M., Morris, R. V., Ming, D. W., & Swayze, G. A. (2010). Silica in a Mars analog environment: Ka'u Desert, Kilauea Volcano, Hawaii. *Journal of Geophysical Research*, *115*, E00D15. https://doi.org/10.1029/2009JE003347

Shean, D. E., Alexandrov, O., Moratto, Z. M., Smith, B. E., Joughin, I. R., Porter, C., & Morin, P. (2016). An automated, open-source pipeline for mass production of digital elevation models (DEMs) from very-high-resolution commercial stereo satellite imagery. *ISPRS Journal of Photogrammetry and Remote Sensing*, *116*, 101–117. https://doi.org/10.1016/j.isprsjprs.2016.03.012

Skok, J. R., Mustard, J. F., Ehlmann, B. L., Milliken, R. E., & Murchie, S. L. (2010). Silica deposits in the Nili Patera caldera on the Syrtis Major volcanic complex on Mars. *Nature Geoscience*, *3*(12), 838–841. https://doi.org/10.1038/ngeo990

Smith, M. R., & Bandfield, J. L. (2012). Geology of quartz and hydrated silica-bearing deposits near Antoniadi Crater, Mars. *Journal of Geophysical Research*, *117*, E06007. https://doi.org/10.1029/2011JE004038

Squyres, S. W., Arvidson, R. E., Ruff, S., Gellert, R., Morris, R. V., Ming, D. W., et al. (2008). Detection of silica-rich deposits on Mars. *Science*, *320*(5879), 1063–1067. https://doi.org/10.1126/science.1155429

Stolper, E. (1982). Water in silicate glasses: An infrared spectroscopic study. *Contributions to Mineralogy and Petrology*, *81*(1), 1–17. https://doi.org/10.1007/BF00371154

Streit, E., Kelemen, P., & Eiler, J. (2012). Coexisting serpentine and quartz from carbonate-bearing serpentinized peridotite in the Samail Ophiolite, Oman. *Contributions to Mineralogy and Petrology*, *164*(5), 821–837. https://doi.org/10.1007/s00410-012-0775-z

Sun, V. Z., & Milliken, R. E. (2015). Ancient and recent clay formation on Mars as revealed from a global survey of hydrous minerals in crater central peaks. *Journal of Geophysical Research: Planets*, *120*, 2293–2332. https://doi.org/10.1002/2015JE004918

Sun, V. Z., & Milliken, R. E. (2018). Distinct geologic settings of opal-A and more crystalline hydrated silica on Mars. *Geophysical Research Letters*, *45*, 10,221–10,228. https://doi.org/10.1029/2018GL078494

Thomas, N. H., & Bandfield, J. L. (2017). Identification and refinement of Martian surface mineralogy using factor analysis and target transformation of near-infrared spectroscopic data. *Icarus*, *291*, 124–135. https://doi.org/10.1016/j.icarus.2017.03.001

Tosca, N. J., & Knoll, A. H. (2009). Juvenile chemical sediments and the long term persistence of water at the surface of Mars. *Earth and Planetary Science Letters*, *286*(3), 379–386. https://doi.org/10.1016/j.epsl.2009.07.004

Ueno, Y., Yoshioka, H., Maruyama, S., & Isozaki, Y. (2004). Carbon isotopes and petrography of kerogens in ~3.5-Ga hydrothermal silica dikes in the North Pole area, Western Australia11Associate editor: G. Cody. *Geochimica et Cosmochimica Acta*, *68*(3), 573–589. https://doi.org/10.1016/S0016-7037(03)00462-9

Wacey, D., Kilburn, M. R., Saunders, M., Cliff, J., & Brasier, M. D. (2011). Microfossils of sulphur-metabolizing cells in 3.4-billion-year-old rocks of Western Australia. *Nature Geoscience*, *4*(10), 698–702. https://doi.org/10.1038/ngeo1238

Werner, S. C. (2008). The early Martian evolution—Constraints from basin formation ages. *Icarus*, *195*(1), 45–60. https://doi.org/10.1016/j.icarus.2007.12.008

Yen, A. S., Ming, D. W., Vaniman, D. T., Gellert, R., Blake, D. F., Morris, R. V., et al. (2017). Multiple stages of aqueous alteration along fractures in mudstone and sandstone strata in Gale Crater, Mars. *Earth and Planetary Science Letters*, *471*, 186–198. https://doi.org/10.1016/j.epsl.2017.04.033